ingegneria sismica
International Journal of Earthquake Engineering
Anno XLIII - Num. 1 - 2026

Research on the Evaluation of Computer-Aided Design-Based Apparel Design Solutions

Ruoheng Du[1] *and Hangshuo Wu*[1,*]

[1] College of Fine Arts and Design, Hebei Institute of Communications, Shijiazhuang, Hebei, 050000, China

SUMMARY: *This paper makes use of the RBF to calculate the interpolated displacement of vertexes on a 3D human body mesh. Through the integration of points of human body landmarks, lines, and customized measurements, a new 3D human body deformation model is created. At the same time, an RBF control point set is formed for the deformation of the 3D human body model. In addition, parametric cubic splines and bicubic surfaces patches are utilized to form a 3D garment model. This approach controls the constraints between 3D model parameters, enabling predictable control over the 3D prototype. Finally, garment design solutions under different methods are compared using SSIM, PSNR, and FID image evaluation metrics. The results show that 3D garment prototypes created using the method successfully imitate prototype designs, proving the usefulness of computer-aided garment designing solutions. The images produced through this method perform extremely well in all aspects and produce the best visual effects in garment designing.*

KEYWORDS: *Radial basis functions; Bicubic surface patches; Three-dimensional garment models; Computer-aided design*

1 Introduction

Computer-Aided Design (CAD) is a vital technology within the development and application of computer science and technology. It leverages computers' rapid numerical computation and powerful graphics processing capabilities to assist engineers, designers, architects, and other technical professionals in product design, engineering drafting, and data management—including tasks such as modeling, calculation, and drafting [1, 2]. CAD has become an indispensable key technology for factories, enterprises, and research institutions to enhance technological innovation capabilities, accelerate product development, and promote rapid growth. It achieves this by improving design quality, speeding up design processes, saving labor and time, and increasing the automation level of design work [3-5]. Supported by CAD, clothing design can be conducted at multiple levels leveraging big data and virtual technologies. Through data mapping, satisfaction levels for different consumer groups can be defined, thereby enhancing design quality [6, 7]. New paradigms for assessing the proposals for designs have been brought about by CAD applications in apparel designing.

In apparel designing, the emergence of CAD technology has brought about significant changes to the traditional design paradigm. This is evident in areas such as styling, fabric selection, pattern-making, and even presentation. The application of software tools in apparel designing has led to efficient processes and enhanced designs. Shaker & Khan (2017) state that

*suzhoudaxue211@163.com
https://doi.org/10.65102/is2026139
Published: 30 April, 2026

in textile designs, the CAD systems are capable of creating simulations in regard to weft thickness and spacing in fabrics using the color rectangles [8]. Yuan et al. (2018) created a CAD model that marked personalized demands (color, pattern, and size) in the CAD outputs in order to create a one-person one piece garment manufacturing process [9]. The process entails the integration of these programmatic designs with CAD, Photoshop, Illustrator, and other similar tools. This ensures that the designs are made without the need for pen and paper; hence, minimizing mistakes that arise from complicated operational processes. These mistakes can be minimized through the software undo options to save on time in the designing process [10-13].

In addition to this, the interactive nature of some aspects offered by the software gives freedom to the designers. Simulation techniques are used to manipulate the accuracy, brightness, and transparency of some patterns. In addition, different types of patterns can be replicated using the computerized pen sketching tool. By adjusting the functions of the software, styles and artistic designs are established based on concepts, bringing out the visibility of the garment design. By entering the body parameters of a human being, digital models that are proportional to humans can be generated. These models facilitate the assessment of the garment designs locally and fully [14-18]. In practice, Rahman et al. (2023) used Huazhong CAD software in analyzing the construction of seamless jackets. The software analyzes the styles and pattern designs of jackets and assesses its performance factors such as yarn and stitch designs, breathability, and elasticity [19]. These factors function as important evaluation criteria in fashion designs. In their study on garment design, Li and Hou (2023) used 3D software called Poser, Computer-Aided Design (CAD), and 3D Max to build 3D digital human models, draft flat pattern for garments, and garment sewing, respectively [20]. The authors created visual effect models using various modeling approaches to evaluate garment design results [20]. In her research, Li (2022) used CAD to develop digital 3D garments suitable for making a sample garment and rendering [21]. The above process ensured that there were visual effects of the models in the computer-aided dyeing system. Jamil and Ijaz (2024) developed unique garment patterns inspired by abstract art through the use of CAD technology. Using tools in Adobe Illustrator and Photoshop, the patterns were applied to garments and viewed in two-dimensional and three-dimensional forms [22].

As technologies such as artificial intelligence make continuous breakthroughs, intelligent functions like smart color matching, pattern creation, and garment layout optimization have been integrated by CAD systems. These continuous improvements contribute positively to the efficiency and aesthetic nature of design, in addition to providing evaluation services for pattern features, colors coordination, and layout of proposed designs. Hu (2021) has analyzed the elements that constitute a garment design and incorporated the use of CAD software in the creation of an intelligent design framework, thus creating an intelligent garment design CAD system [23]. Liu (2023) has extracted 3D texture features from images captured from various light directions and applied machine learning classification in the identification of image features. The incorporation of emotional aspects in the process has been achieved using the CAD system in apparel design and services [24]. Chen & Zang (2024) have used data mining technology in the development of a threshold segmentation technique for graphic design images, allowing the extraction of pattern features from the CAD software system [25]. Wang & Chen (2024) applied deep learning technology in the creation of aerospace Arisa apparel design CAD software, using deep convolutional neural network to extract stylistic features of images, and then incorporate texture features using transfer learning [26].

The aforementioned CAD technologies all change conventional methods of design, presentation, and evaluation of fashion. Conventionally, the evaluation is usually dependent on subjective aesthetics of the designers themselves without objective and standard criteria. Digital technology can offer objective and precise evaluation process. With CAD technologies, three-

dimensional evaluations become possible, including assessments of fabric properties, pattern color schemes, seam placements, and aesthetics of the designs.

The present paper aims at the evaluation of the effect produced by clothing design schemes under computer-aided design. First, radial basis function interpolation is adopted to deal with deformation displacements on all feature curves of the human body, thus allowing for precise deformations of the triangular mesh of the human body. Then, a three-dimensional clothing prototype model will be constructed based on cubic spline curves and bicubic surfaces that are controlled by endpoint coordinates, endpoint tangent vectors, and parameters of endpoint tangent vectors. The similarity between synthesized images and original images will be evaluated using Peak Signal-to-Noise Ratio (PSNR), Structural Similarity Index (SSIM), and FID. Subsequently, the computer-aided design proposals are evaluated based on varying distortion angles, line widths, and color fill aspects. Finally, design samples generated by this method were compared with other models, further validating the superiority and effectiveness of the proposed approach.

2 Computer-Aided Design-Based Apparel Design Methodology

2.1 Deformation Algorithms for Three-Dimensional Human Models

Personalized human body model creation requires the use of spatial deformation techniques. Spatial deformation means the distortion and deformation of the geometric object into particular shapes while maintaining their topological structure during the deformation process. In the process of parameterizing the human body model, the model will be segmented into different sections according to predetermined morphological features. With changes in the value of the morphological parameter, the system will automatically manipulate the length, circumference, or width of different body sections to get the desired shape of the human body model.

This paper generates human models of varying sizes by deforming a human template, preparing for the construction of 3D garment prototypes. The deformation problem of the human model is transformed into the deformation of its triangular mesh. We employ radial basis functions (RBFs) [27] to interpolate the deformation displacements of all feature curves on the human body, thereby achieving deformation of the triangular mesh. The advantage of this deformation method lies in solving a single set of equations for all feature control points without requiring mesh connectivity information, enabling highly precise and efficient mesh deformation.

2.1.1 Deformation Methods for Human Models

(1) Radial Basis Function Theory

Radial basis functions enable smooth interpolation of point set displacements. Given the displacements of several control points, this method determines the displacements of the remaining mesh vertices. If the values of a scalar function $F_i : R^3 \to R$ at N distinct points p_i in three-dimensional space are known, the radial basis function can be described as:

$$F(p) = \sum_{i=1}^{M} a_i g(\| p - p_i \|) + c_0 + c_1 x + c_2 y + c_3 z \quad (1)$$

Here, $F(p)$ denotes the displacement interpolation of point $p=(x,y,z)$ in three-dimensional space. $p_i=(x_i,y_i,z_i)$ represents the RBF control point, and a_i is the interpolation weight coefficient. The final four coefficients c_0,c_1,c_2,c_3 describe a rigid body transformation not achievable via RBF, while $g(\| p-pi \|)$ is a basis function concerning the Euclidean distance between points p and p_i.

(2) Mesh Deformation

By applying the interpolation function $F(p)$ to describe the displacement of each point in 3D space based on the displacement of given RBF control points, the displacement of each vertex in the mesh model can be obtained.

Let the displacement of any RBF control point be denoted as $u_i=(\Delta x_i,\Delta y_i,\Delta z_i)$ and $F(p_i)=u_i$, the RBF interpolation function can be expressed as the following system of linear equations:

$$\begin{aligned} GA_x &= (\Delta x_1,\Delta x_2,\cdots\Delta x_N,0,0,0,0)^T \\ GA_y &= (\Delta y_1,\Delta y_2,\cdots\Delta y_N,0,0,0,0)^T \\ GA_z &= (\Delta z_1,\Delta z_2,\cdots\Delta z_N,0,0,0,0)^T \end{aligned} \tag{2}$$

where G is an $(N+4)\times(N+4)$ matrix:

$$\begin{bmatrix} g_{11} & g_{12} & \cdots & g_{1N} & 1 & x_1 & y_1 & z_1 \\ g_{21} & g_{12} & \cdots & g_{1N} & 1 & x_2 & y_2 & z_2 \\ \cdots & \cdots & \cdots & \cdots & \cdots & \cdots & \cdots & \cdots \\ g_{N1} & g_{N2} & \cdots & g_{NN} & 1 & x_N & y_N & z_N \\ 1 & 1 & \cdots & 1 & 0 & 0 & 0 & 0 \\ x_1 & x_2 & \cdots & x_N & 0 & 0 & 0 & 0 \\ y_1 & y_2 & \cdots & y_N & 0 & 0 & 0 & 0 \\ z_1 & z_2 & \cdots & z_N & 0 & 0 & 0 & 0 \end{bmatrix} \tag{3}$$

In the matrix, $g_{ij}=g(\| p_i-p_j \|)$, where p_i and p_j are RBF control points. A_x is the coefficient matrix for a_i in the x-coordinate of the 3D vertex, A_y is the coefficient matrix for a_i in the y-coordinate of the 3D vertex, and A_z is the coefficient matrix for a_i in the z-coordinate of the 3D vertex, as shown below.

$$\begin{aligned} A_x &= \begin{bmatrix} a_{x_1} & a_{x_2} & \cdots & a_{x_N} & c_0 & c_1 & c_2 & c_3 \end{bmatrix}^T \\ A_y &= \begin{bmatrix} a_{y_1} & a_{y_2} & \cdots & a_{y_N} & c_0 & c_1 & c_2 & c_3 \end{bmatrix}^T \\ A_z &= \begin{bmatrix} a_{z_1} & a_{z_2} & \cdots & a_{z_N} & c_0 & c_1 & c_2 & c_3 \end{bmatrix}^T \end{aligned} \tag{4}$$

By solving the system of equations, the solutions A_x,A_y,A_z are obtained, enabling the calculation of the interpolated displacement in three-dimensional space for all three-dimensional vertices.

2.1.2 Deformation Implementation for Human Models

(1) Establishment of RBF Control Points

To achieve accurate and efficient deformation of the human body model, this paper establishes a compact set of RBF control points by combining points on both feature points and feature lines. When implementing lengthwise deformations such as height, arm length, and leg length, it is necessary to obtain the displacement of points on both feature points and feature lines. In contrast, circumferential deformations only require the displacement of points on feature lines. The four selected control points include the vertex point, acromion point, foot point, and neck point.

For obtaining RBF control points that are used to perform circumferential dimension deformation, first a 3D transformation technique is applied to transform the circumferential point set, which is formed using the intersection of the tangent plane and the human model's surface patches, into the XOY plane. Following this step, the adjacent points within the point set are sequentially connected to form the circumferential polygon of the point set. Next, the center point of the circumference point set is selected as the reference point, serving as the center of the unit circle. The circumference of the unit circle is divided into X equal segments based on its circumference length, where X represents the number of RBF control points on that circumference line. Finally, the intersection points between each ray from the unit circle center to the equidistant points and the boundary of the circumference polygon are determined. These intersection points serve as the RBF control points for the circumference dimension line. The RBF control points and their displacements are illustrated in Figure 1, where (a) shows the chest circumference polygon and RBF control points, and (b) depicts the displacement of the chest circumference RBF control points. Once RBF control points are established for all circumferences, the RBF dimensional control model for the human body is complete.

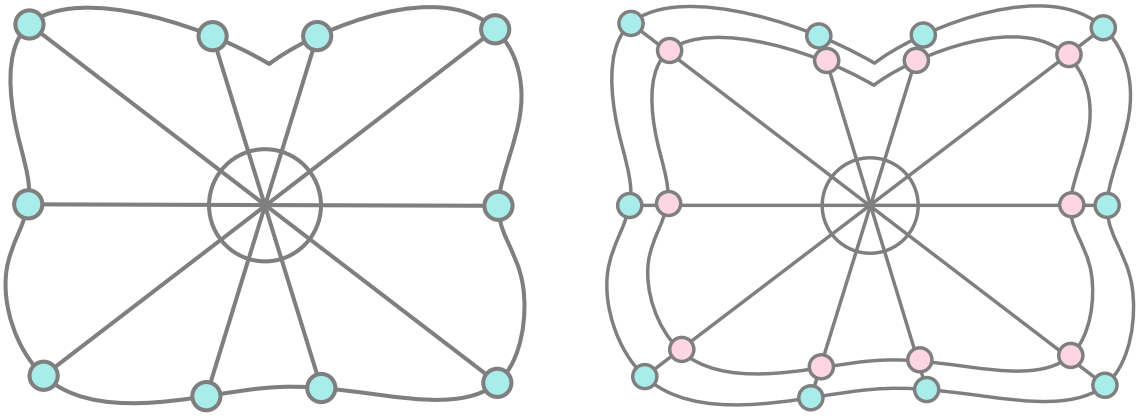

(a)Multimodal chest wall and RBF control points

(b) Movement of RBF control points around the chest

Figure 1: RBF control points and their displacement

(2) Implementation of Personalized Human Body Parameter Modeling

By calculating the displacement of RBF control points, we can compute the interpolated displacement of vertices on the human body mesh. This enables the generation of new human body models based on user-specified dimensions. The displacement calculation for RBF control points on circumference feature lines involves first radially moving vertices along the circumference curve in the XOY plane. The desired circumference dimension is approximated by calculating the length of the convex hull of these vertices. Once radial vertex movement achieves the specified circumference dimension, the distance between a new point on the same

circumference ray and a point on the human template circumference serves as the displacement for that control point. For displacement calculation of RBF control points along the length dimension, feature control points and circumference line control points are proportionally distributed along the length dimension. The displacement of these control points directly corresponds to their displacement along the length dimension.

2.2 Three-Dimensional Garment Prototype Construction Method Based on Key Value Point Control

The preceding section performed a 3D reconstruction of the human body model. On the basis of this model of a 3D human body, a model of a 3D garment is created on the principle of controlling key points. Creating a 3D garment model requires five stages:

1) Studying the form of the 3D garment, forming its 3D mathematical model for different parts of the garment, and selecting key points that control changes in the model.

2) According to the location of the 3D garment model relative to the 3D human model, capturing the coordinates of each key shape point directly through the method of capturing 3D data points.

3) Establishing parameters of each key shape point based on ergonomics and structural characteristics of garments.

4) Construct the 3D garment prototype using cubic spline curves and bicubic surfaces based on the determined parameters.

When selecting key shape points, prioritize the following conditions to facilitate parameter control:

(1) The tangent direction at the shape point along the line forming the prototype must be perpendicular or parallel to one of the axes in the 3D coordinate system.

(2) The point is a critical shape value point controlling the form of the three-dimensional garment prototype. Utilize the key lines determined by these points to perform quadrilateral surface subdivision on the garment's three-dimensional form.

2.2.1 Methods for Establishing Three-Dimensional Garment Wireframe Models

To achieve intelligent control of three-dimensional prototypes, this paper employs cubic spline curves controlled by endpoint coordinates, endpoint tangent vectors, and endpoint tangent vectors [28], along with bicubic surfaces, to construct three-dimensional garment models.

Let $p_i(u)$ denote the equation of the i-th segment of the spline curve, then we have:

$$p_i = A_3u^3 + A_2u^2 + A_1u + A_0; \quad u \in [0, L_i] \tag{5}$$

Among these, L_i denotes the chord length of the ith segment of the curve.

The geometric matrix form of $p_i(u)$ is:

$$p_i(u) = \begin{bmatrix} u^3 & u^2 & u^1 & u \end{bmatrix} \begin{vmatrix} 2/L_i^3 & -2/L_i^3 & 1/L_i^2 & 1/L_i^2 \\ -3/L_i^2 & 3/L_i^2 & -2/L_i & -1/L_i \\ 0 & 0 & 1 & 0 \\ 1 & 0 & 0 & 0 \end{vmatrix} \begin{vmatrix} p_{i-1} \\ p_i \\ M_{i-1} \\ M_i \end{vmatrix} \tag{6}$$

Here, P_i and P_{i-1} denote the coordinates of the endpoints of the ith segment of the curve, while M_i and M_{i-1} denote the tangent vectors at the endpoints of the curve.

2.2.2 Methods for Establishing Three-Dimensional Garment Surface Models

After establishing the three-dimensional garment wireframe model, this paper employs double cubic surface patches to construct the three-dimensional garment surface model.

The algebraic form of the double cubic surface patch is:

$$p(u,w)=\sum_{i=0}^{3}\sum_{j=0}^{3}a_{ij}u^{i}w^{j}\quad (u,w)\in[0,1] \tag{7}$$

Among these, two parameters are defined on the interval [0, 1], and a_v is referred to as the algebraic coefficient of the surface.

The geometric matrix form of a bicubic surface patch is:

$$\begin{aligned} p(u,w)&=[F_1(u)F_2(u)F_3(u)F_4(u)]\begin{vmatrix} p_{00} & p_{01} & p_{00}^{w} & p_{01}^{w} \\ p_{10} & p_{11} & p_{10}^{w} & p_{11}^{w} \\ p_{00}^{w} & p_{01}^{w} & p_{00}^{ww} & p_{01}^{ww} \\ p_{10}^{w} & p_{11}^{ww} & p_{10}^{ww} & p_{11}^{ww} \end{vmatrix}\begin{vmatrix} F_1(w) \\ F_2(w) \\ F_3(w) \\ F_4(w) \end{vmatrix} \\ &=F(u)BF(w)^{T} \\ &=UMBM^{T}W^{T} \end{aligned} \tag{8}$$

where $F(u)=UM$, $F(w)=WM$, $U=[u^3u^2u^1]$, $w=[w^3w^2w^1]$, M shares the same coefficient matrix as the cubic Hermite curve:

$$M=\begin{bmatrix} 2 & -2 & 1 & 1 \\ -3 & 3 & -2 & -1 \\ 0 & 0 & 1 & 0 \\ 1 & 0 & 0 & 0 \end{bmatrix} \tag{9}$$

It can thus be seen that the primary task in constructing a parametric surface is to determine its geometric coefficient matrix B. Given the equations of the four boundary curves of the surface patch as $p_{0w}, p_{1w}, p_{u0}, p_{u1}$. The first two rows of matrix B are filled using the geometric coefficients of curves p_{0w} and p_{1w}:

First row: $p_{0w}\rightarrow p_{00}\ \ p_{01}\ \ p_{00}^{w}\ \ p_{01}^{w}$;

Second row: $p_{1w}\rightarrow p_{10}\ \ p_{11}\ p_{10}^{w}\ p_{11}^{w}$

Fill the first two columns of the matrix with the geometric coefficients of curves p_{u0} and p_{u1}:

First column: $\begin{matrix} p_{u0}^{u} \\ \downarrow \\ p_{p_{00}} \\ p_{10} \\ p_{00} \\ p_{10} \end{matrix}$, the second column $\begin{matrix} p_{n-1}^{n} \\ \downarrow \\ p_{01} \\ p_{11} \\ p_{01} \\ p_{11} \end{matrix}$.

Thus, the 12 vectors in matrix B can be determined. Dividing matrix B into four quadrants, the four vectors in the upper left quadrant define the four corner points. The four vectors in the upper right quadrant contain the tangent vectors to the corners with respect to w. The four vectors in the lower left quadrant contain the tangent vectors to the corners with respect to u. The four vectors in the lower right quadrant are the twist vectors (mixed partial derivatives) at the corners. The first three sets of information fully determine the positions and shapes of the four boundary curves. The fourth set of corner twistors bears no relation to the boundary shape; instead, it reflects the surface's convexity or concavity. Geometrically, it represents the rate of change of the tangent vector in the w-direction along the u-direction, or the rate of change of the tangent vector in the u-direction along the w-direction near the corner point. When the corner twistor equals zero, the surface becomes quite flat near that point.

Among bicubic surface sheets, a special class of parametric surfaces are straight-line surfaces: surfaces formed by the trajectory of a straight line moving with one degree of freedom, such that at least one straight line passes through every point on the surface. Given two boundary curves p_{u0} and p_{u1}, a straight-line surface is formed by connecting points with identical u-values on these curves via straight lines. The corresponding equation is:

$$Q(u,w) = p(u,0)(1-w) + p(u,1)w \tag{10}$$

Given p_{0w} and p_{1w}, the straight-grained surface can be expressed as:

$$Q(u,w) = p(0,w)(1-u) + p(1,w)u \tag{11}$$

2.3 Evaluation Methods for Apparel Prototype Design Outcomes

2.3.1 SSIM

SSIM is a metric for measuring image similarity, utilizing a combination of three aspects—luminance, contrast, and structure—as visual information of an image. For instance, it utilizes the mean to estimate the luminance, the standard deviation to estimate the contrast, and the covariance to evaluate the structural similarity. Given an original image x and a distorted image y, the SSIM calculation can be expressed as below:

$$SSIM(\mathrm{x},y) = \frac{(2\mu_x\mu_y + c_1)(2\delta_{xy} + \delta_2)}{(\mu_x^2 + \mu_y^2 + c_2)(\delta_x^2 + \delta_y^2 + c_2)} \tag{12}$$

In the formula: μ_x、μ_y are the respective mean values of images x and y; δ_x^2、δ_y^2 are the respective variances of x and y; δ_{xy} is the covariance between x and y; c_1、c_2 are constants to maintain stability, $c_1=(k_1L)^2, c_2=(k_2L)^2$ where L is the luminance dynamic range, and $k_1 = 0.01, k_2 = 0.05$. c_1、c_2 ranges from 0 to 1. When two images are identical, SSIM equals 1; when no relationship exists, SSIM equals 0. A higher SSIM value indicates greater similarity between images in brightness, contrast, and structure, meaning the processed image is perceptually closer to the original.

2.3.2 PSNR

Peak Signal-to-Noise Ratio (PSNR) and Structural Similarity Index (SSIM) are both used to quantify image quality, but they assess it from different perspectives. PSNR measures image

quality by calculating the ratio of the signal's peak value to the root mean square error between the signal and noise. That is, PSNR is computed by comparing pixel-level differences between the original image and the compressed or processed image. A higher PSNR value indicates smaller differences between images, meaning the compressed or processed image is more similar to the original.

The PSNR formula is:

$$PSNR = 10.\log_{10}(\frac{MAX_1^{\ 2}}{MSE}) \tag{13}$$

MAX_1 represents the maximum grayscale value of the denoised signal, and the magnitude of MAX_1 determines the maximum grayscale bit depth of the signal. MSE (mean square error) is the mean square error, defined by the following formula:

$$MSE = \frac{1}{ab}\sum_{i=0}^{a-1}\sum_{j=0}^{b-1} \| H(i,j) - G(i,j) \|^2 \tag{14}$$

In the equation, $H(i,j)$ and $G(i,j)$ denote the corresponding grayscale values and color values on the original and reconstructed pixels, respectively, while $(a-1)$ and $(b-1)$ represent the number of pixels, which is $(a \cdot b)$ pixels.

2.3.3 FID

FID is an image evaluation metric proposed in recent years that considers not only the distribution of synthetic images but also how to compare it with the distribution of real data. It directly measures the distance between the synthetic data distribution $p(\bullet)$ and the real data distribution $p_r(\bullet)$. In practice, images are encoded using visual features by the Inception model. Assuming feature embeddings follow a multivariate Gaussian distribution, the Gaussian mean and variance (m, C) of the synthetic data are obtained from the synthetic data distribution $p(\bullet)$, while the Gaussian mean and variance (m_r, C_r) of the real data are obtained from the real data distribution $p_r(\bullet)$. The difference between the Gaussian distributions of the synthetic data and the real data is calculated using the following formula:

$$FID = \| m - m_r \|_2^{\ 2} + T_r(C + C_r - 2(CC_r)^{1/2}) \tag{15}$$

The lower the FID value, the smaller the distance between real data and synthetic data.

3 Effect Evaluation of Computer-Aided Design-Based Apparel Design Solutions

3.1 Simulation of Apparel Design Effects Using Computer-Aided Design

This study examines three stand-up collar designs, with Collar Style 1 composed of cotton and Collar Styles 2 and 3 composed of synthetic fibers. The design outcomes were simulated in three dimensions using the methodology presented herein, followed by experimental validation of the results. The study participants comprised 100 first-year design majors from XXX School.

3.1.1 Fabric Sample Performance Parameters

The performance parameters of the fabric samples are shown in Table 1. The results indicate that the two fabrics are composed of cotton and synthetic fiber respectively, both with a twill weave structure. The specific warp density, weft density, thickness, and mass are as follows.

Table 1: Fabric sample performance parameters

Number	Ingredient	Organization structure	Diameter (root/10cm)	Density (roots/10cm)	Thickness (mm)	Weight (mg/cm^2)
①	Cotton	Twill	485	362	0.32	22.34
②	Chemical fiber	Twill	455	299	0.71	31.51

3.1.2 Analysis of Actual Verification Results for Collars

The actual design drawings of the three stand-up collars are shown in Figure 2, where (a) to (c) represent three different stand-up collar styles respectively.

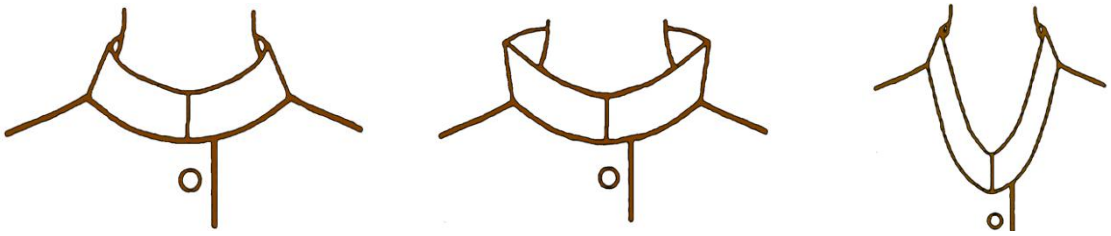

(a)Style 1 of the uniform (b) Style 2 of the uniform (c) Style 3 of the uniform

Figure 2: Three kinds of practical design drawings of collar

The 3D simulation results for three stand-up collar styles are shown in Figure 3, where (a) to (c) represent three distinct collar designs. The three lines in the figure correspond to cubic spline curves controlled by endpoint coordinates, endpoint tangents, and endpoint torsions, respectively. The results demonstrate that after applying three-dimensional deformation to the human model parameters described herein, the three-dimensional garment prototype constructed using key value point control effectively simulates the prototype designs of the three stand-up collars. The method meets the needs for computer-aided design combined with pattern generation through images. It shows that computer-aided design models can automatically create clothes according to the human body and style characteristics, making contributions to studies on 3D digital garments. Based on these theoretical and experimental studies, it offers guidance for the ultimate goal of computer-based generation of clothing patterns based on individual body shapes.

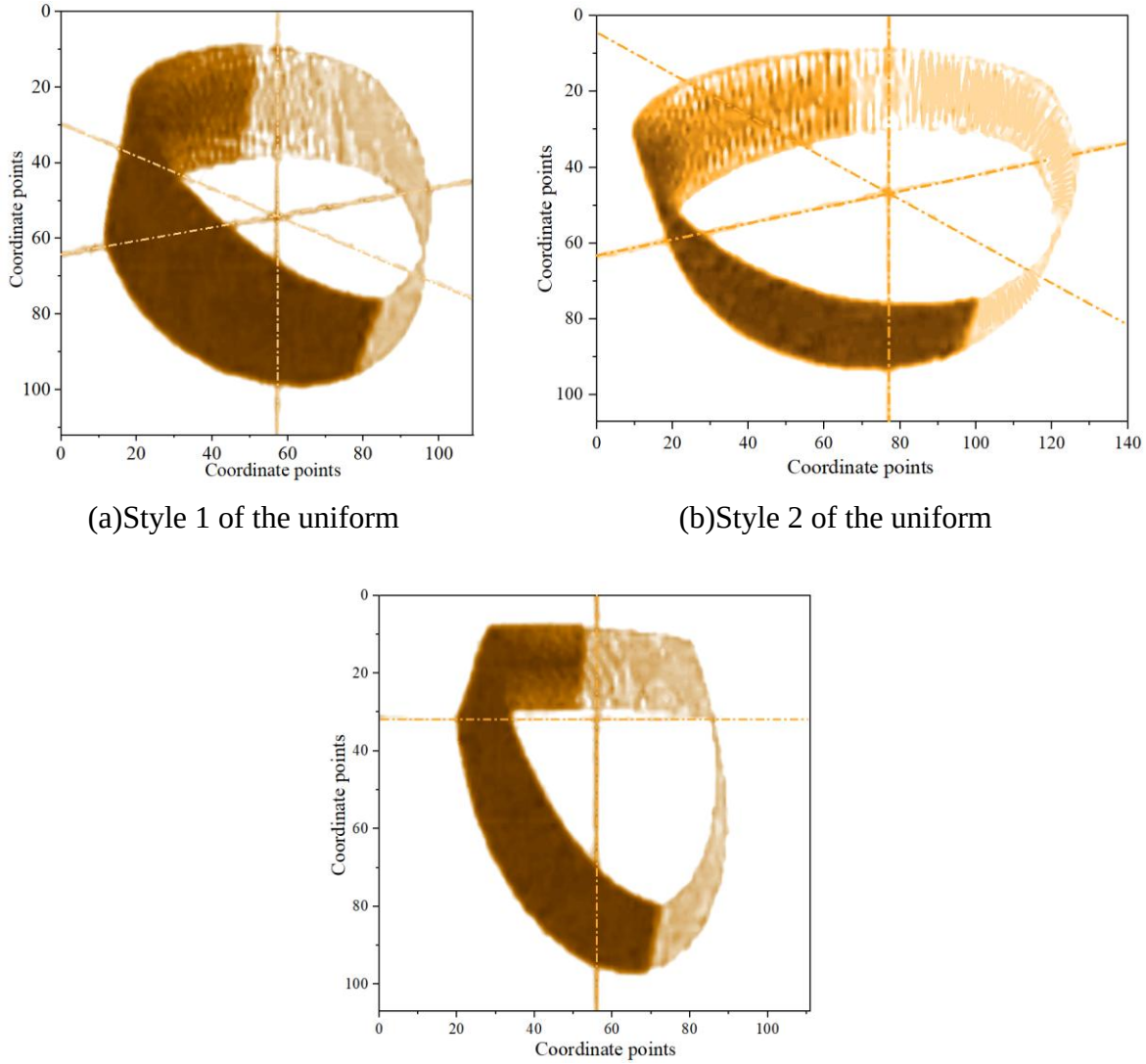

(a)Style 1 of the uniform

(b)Style 2 of the uniform

(c)Style 3 of the uniform

Figure 3: Three-dimensional simulation results of three kinds of collar

3.2 Performance Evaluation of Garments Designed Using Different Methods

For the comprehensive validation of the efficacy of the proposed methodology against traditional design methodologies (LoRA model, ControlNet, and hand-drawn designs), experimental tests were performed. The FID (Fresher Initial Distance) criterion was utilized for the comparison of the similarity of generated images with original images. This metric determines the extent of similarity according to the prompt description. Moreover, SSIM (Structural Similarity Index) and PSNR (Peak Signal-to-Noise Ratio) criteria were used for the determination of the quality of generated images.

Table 2 illustrates the comparative performance results of different design techniques applied in clothes design. According to the results, there is a notable difference between the performance of the methods. The proposed technique delivered outstanding results according to all the criteria used in the research: it demonstrated the highest similarity in terms of FID (the maximum value was 63.0221), the best image quality (the maximum PSNR of 52.9133), and the best structural similarity (SSIM of 0.9802). In comparison, the LoRA model performs a

little bit worse, with an FID value of 69.4744, a PSNR value of 52.8289, and an SSIM value of 0.9577, suggesting that the generated images have slightly worse similarity and quality than our method. The control net model generates images with similar but slightly worse similarity and quality than our method and even the LoRA model. The hand-drawn designs have the worst performance on the four metrics, achieving the poorest similarity and quality of the generated images, which verifies the validity of the proposed algorithm. In conclusion, the generated images of the clothes produced by this approach are highly consistent with the characteristics of the garment style and color, which indicates that clothes prototypes designed based on human body deformation can achieve great success.

Table 2: Design clothing performance comparison by different methods

Empirical method	FID	SSIM	PSNR
The methodology of this paper	63.0221	52.9133	0.9802
LoRA model	69.4744	52.8289	0.9577
ControlNet method	65.4929	50.1859	0.9002
Hand-drawn design	78.5845	49.06	0.8706

3.3 Effect Evaluation of Computer-Aided Apparel Design Solutions

Experimental Materials Selection: In order to study the influence factors of visual attention, computer aided design (CAD) images of illusion clothes were classified by design parameter into three categories. (1) First Category: The experimental materials with different distortion angles, see Figure 4. (2) Second Category: The experimental materials with different line widths, see Figure 5. (3) Third Category: The experimental materials with different colors, see Figure 6. It is found that there are 12 experimental group images when we grouped 9 experimental images with same rotation angle but different line width together. There are 9 experimental group images when we grouped 12 experimental images with same line width but different distortion angle together. There are 14 experimental group images when we grouped 6 experimental images with same line width and distortion angle but different colors together.

The experimental device chosen was the EYE LINK 1000 desktop eye tracker, with the sampling rate being 1050 Hz and the fixation accuracy being 0.2° -0.6°, which made its spatial resolution excellent. The experiment frame was built using Experiment Builder software, and the eye tracking data could be analyzed and exported using EyeLink DataViewer.

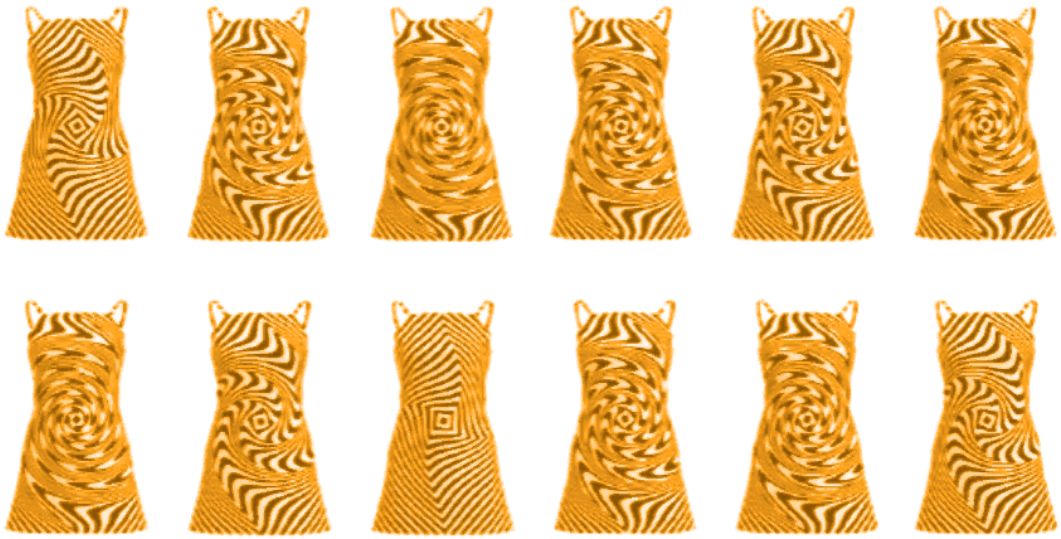

Figure 4: Experimental samples at different rotation angles

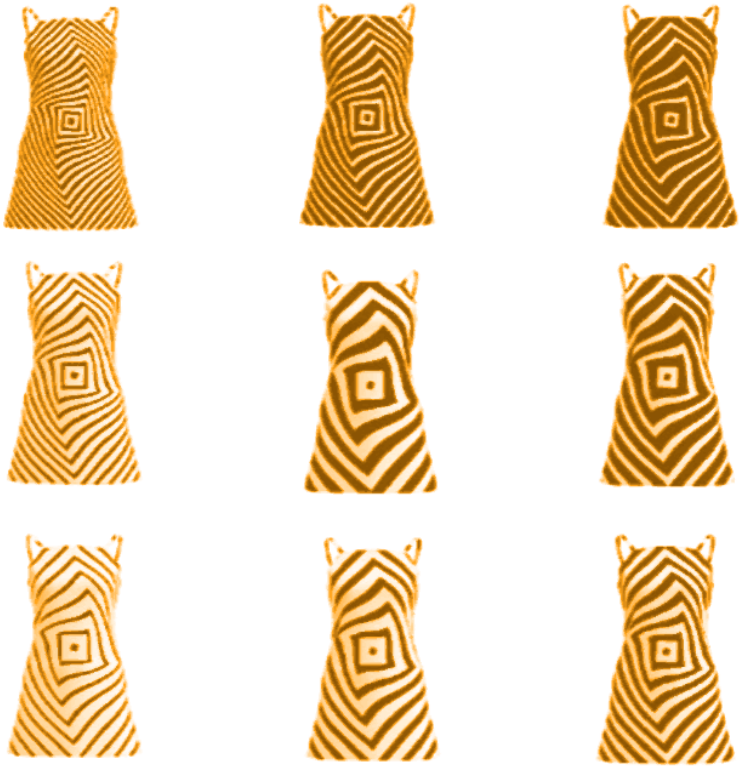

Figure 5: Experimental samples of different line widths

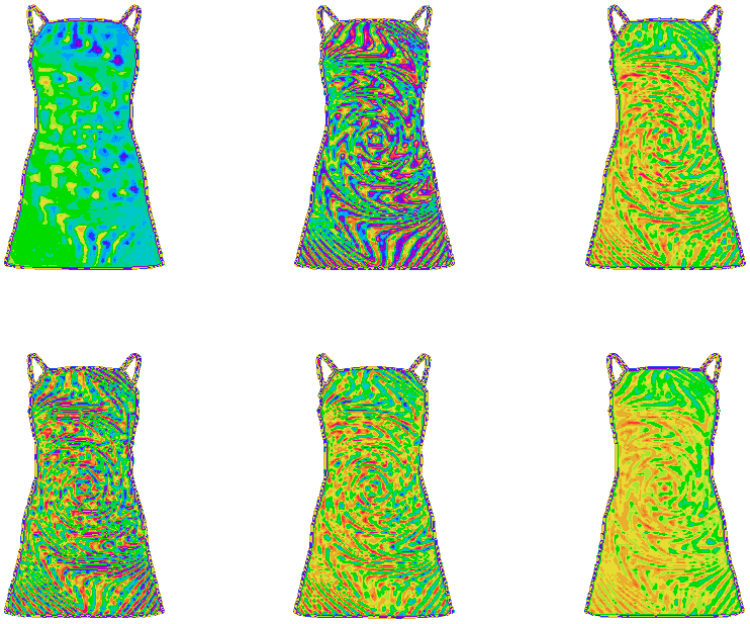

Figure 6: Experimental samples in different colors

3.3.1 Visual Distortion Effects in Fashion Design at Different Angles

Experiment 1 comprised 9 experimental samples, each consisting of 12 optical illusion clothing images featuring identical line widths but varying distortion angles. Each optical illusion image was divided into one region of interest, yielding a total of 108 regions of interest.

(1) Analysis of Mean Pupil Size: To investigate eye movement differences when subjects viewed optical illusion clothing with varying distortion angles, the mean pupil sizes across all

subjects for each region of interest during sample viewing were statistically compiled. Subject mean pupil sizes/units are shown in Figure 7. It can be observed that within the same experimental image set, the distribution of mean pupil sizes across different regions of interest is scattered with no discernible pattern. That is, within the same image, at the same line width, changes in distortion angle did not significantly stimulate pupil size in subjects. Therefore, the entire experimental image set underwent mean normalization. Horizontal comparisons were made using the mean pupil size of each experimental image set to analyze the effectiveness of visual illusion clothing image designs with different distortion angles under computer-aided design.

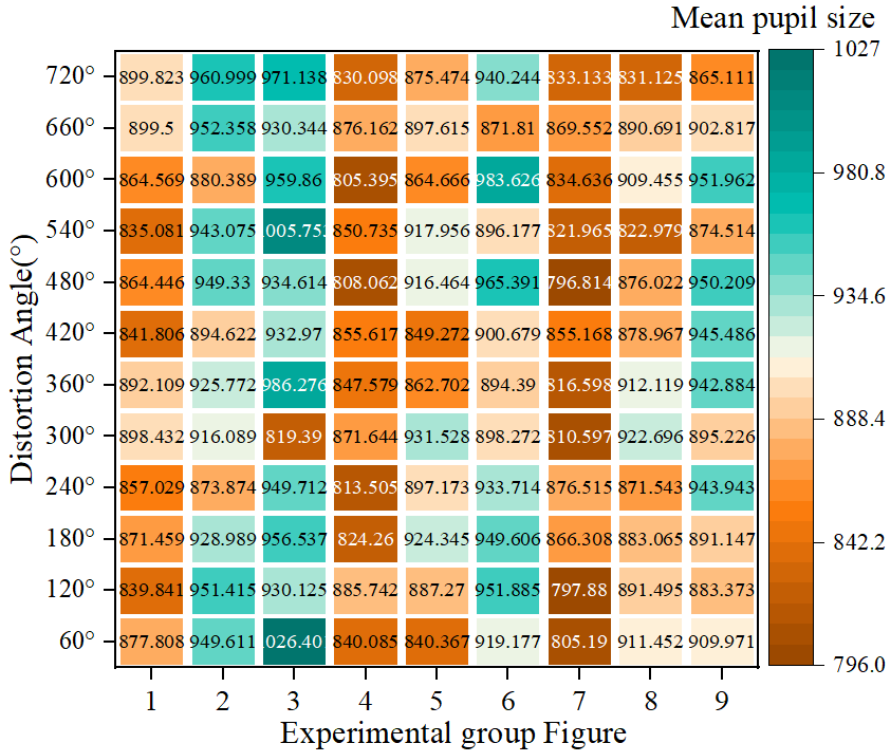

Figure 7: Mean pupil size of subjects/units

Figure 8 shows the mean pupil sizes corresponding to different line widths. The distribution of mean pupil sizes in the figure reveals a consistent pattern every three points. The three points within the blue circle have horizontal coordinates of 1:1, 1:2, and 1:3, with vertical coordinates increasing accordingly. This indicates that for the same width of the brown line (experimental sample), wider lines result in larger pupil sizes when subjects view the distorted optical illusion clothing. The other three dots inside the yellow circle have their horizontal axis measurements as 1:3, 2:3, and 3:3 respectively while their vertical axis measurements decrease progressively. It shows that the bigger the yellow line width is while the brown line width remains constant, the smaller the size of the pupil becomes in the subjects. The largest pupil size occurs during the observation of brown-yellow lines in a width ratio of 1:3 while the smallest occurs during the observation of the width ratio of 3:1.

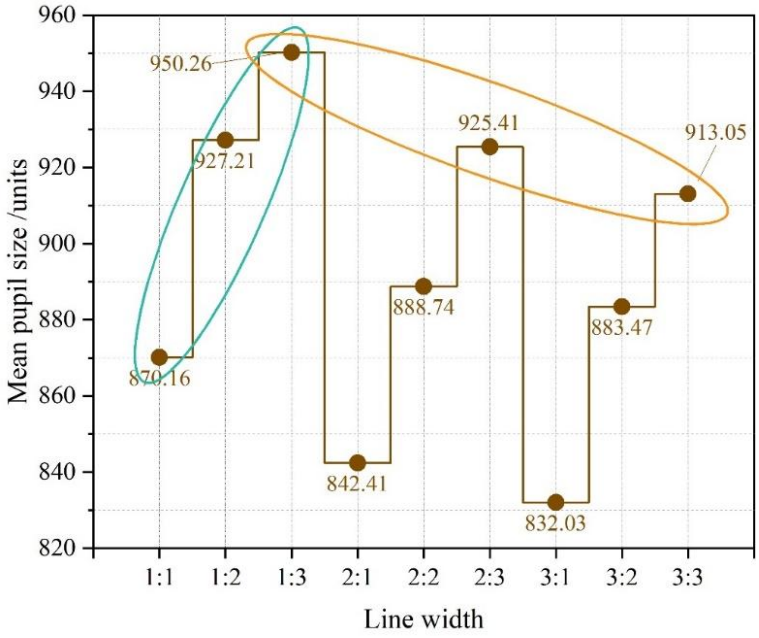

Figure 8: Mean pupil size corresponding to different line widths

(2) Analysis of the First Gaze Duration: Figure 9 shows the first gaze duration associated with various distortion angles. When the line width remains constant, the mean duration of the first gaze is greatest and smallest when the distortion angle is 180° and 360°, respectively. The mean amplitude of the first scan is greatest when the distortion angle is 420°, while the lowest mean amplitude of the first scan is when the distortion angle is 720°. This indicates that designers may select the appropriate garment designs with various distortion angles using computers and determine their first gaze durations.

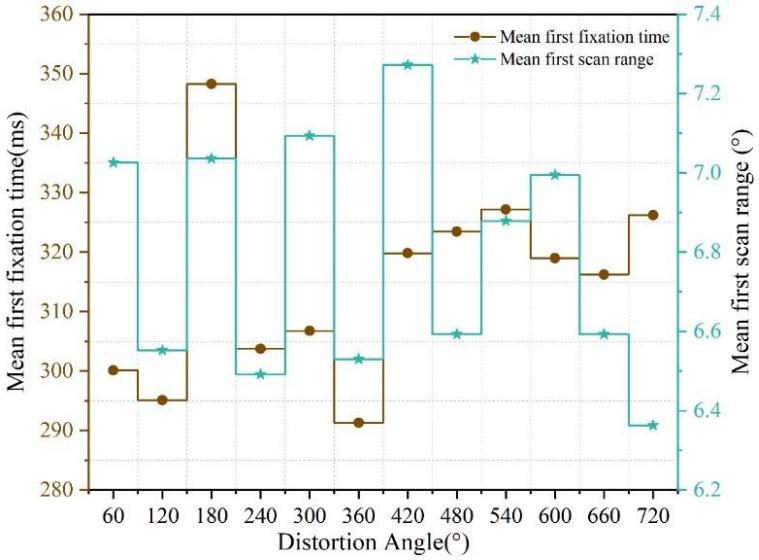

Figure 9: First viewing metrics for different distortion angles

3.3.2 Visual Illusion Effects in Clothing Design with Different Line Widths

The experimental samples in Experiment 2 originated from the same source as those in Experiment 1.

(1) Analysis of mean pupil size: The mean pupil sizes corresponding to different distortion

angles are shown in Figure 10, where 1–12 represent the 12 experimental samples. The distribution of mean pupil sizes exhibits a certain correlation with distortion angle. Overall, as the distortion angle increases, the mean pupil size also increases. As the distortion angle increases, the pupil size of subjects viewing the garment image also increases. This further demonstrates that computer-aided design garment samples can more efficiently assist designers in screening visual error garment images, thereby enhancing the efficiency of the visual error garment image selection process in garment sample design.

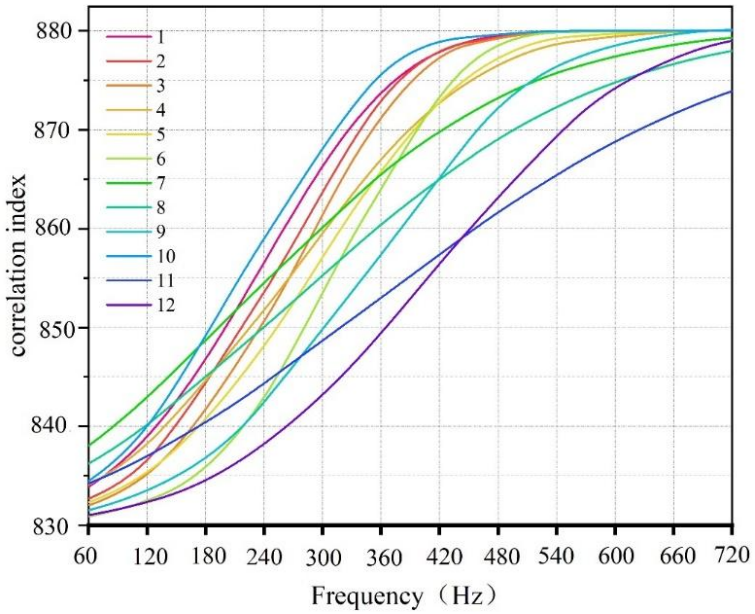

Figure 10: Mean pupil size corresponding to different distortion angles

(2) Initial Viewing Metrics Analysis: Analyzed participants' first fixation duration and initial saccade amplitude when viewing optical illusion clothing images with varying line widths. Initial viewing metrics corresponding to different distortion angles are shown in Figure 11. A 3:1 line width most likely resulted in the longest initial fixation duration when participants first viewed the optical illusion clothing images. A 1:3 line width yielded the largest mean initial saccade amplitude. This indicates that subjects were willing to scan the 1:3 line width optical illusion clothing image with greater amplitude during their first viewing. Since computer-aided design offers greater simplicity and efficiency in adjusting sample line width details, this significantly aids subjects in more quickly selecting preferred samples when viewing optical illusion clothing images with varying line widths. Consequently, it assists designers in obtaining optimal design solutions more rapidly.

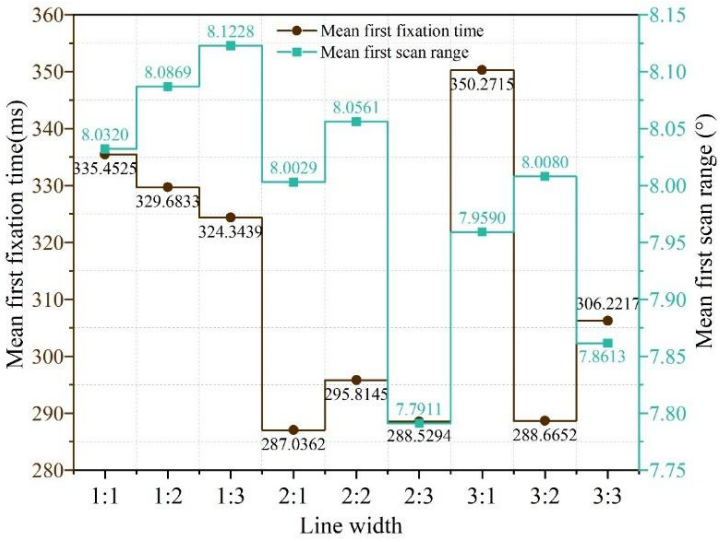

Figure 11: First viewing metrics for different distortion angles

3.3.3 Visual Illusion Effects in Fashion Design with Different Color Fillings

Experiment 3 comprised 14 experimental samples, with each experimental group image containing 6 regions of interest, yielding a total of 84 regions of interest. These corresponded to 84 different color-filled optical illusion patterns.

The mean pupil sizes corresponding to different R, G, and B values are shown in Figure 12. These represent the mean pupil sizes of participants when two of the three R, G, and B values were set to 0, while the third value varied. Results indicate that mean pupil size variations correlate with RGB values. The mean pupil sizes of G values mostly lie within the range of 825-900 since the colors used are highly concentrated in the clothing illusion pictures. The range of distribution for R and B values is mostly 775-925 and 800-950 respectively. The most concentrated fill colors of G and B values have similar size whereas the R value fill color was slightly bigger in size. The color filling for the apparels design is one of the very essential components of the design proposal. Yet the variation of colors brings about complications. This research makes use of computer aided apparel design for quick comparison of design proposals in terms of color filling.

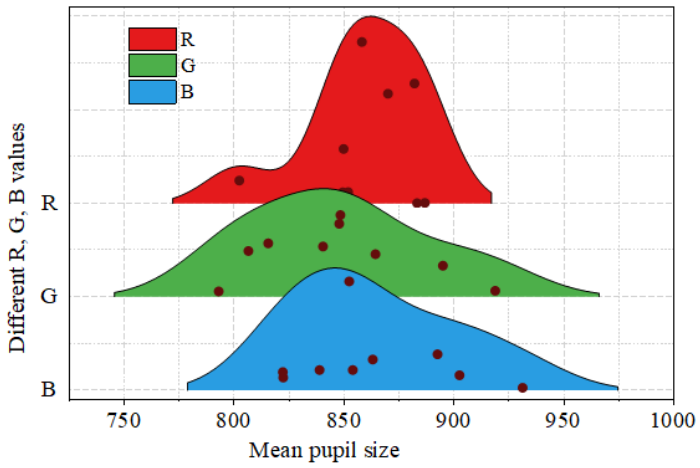

Figure 12: Mean pupil size corresponding to different R, G and B values

4 Conclusion

This study first conducts a 3D deformation process on a human body model and then designs a 3D garment prototype through cubic splines and bicubic surface patches. Finally, image evaluation techniques are used to analyze the CAD images of the garments.

It can be concluded from the findings that:

(1) The CAD system is able to automatically design garments according to human body and style parameters, which contributes to 3D garment technology research and offers a basis for the future creation of computer-designed garment patterns for individual bodies.

(2) Subjects' attention to garment design images is influenced by image distortion angle, line width, and fill color. For instance, when the brown lines in optical illusion patterns are wider, the distortion angle is greater, and the fill color is lighter, subjects spend more time gazing at the patterns, indicating higher attention to the garment design samples and better design effectiveness.

(3) The generated images achieved values of 63.0221 for FID, 52.9133 for PSNR, and 0.9802 for SSIM. These metrics indicate the highest similarity to the original images and the best image quality among all generated images.

About the Author

Ruoheng Du was born in Zibo, Shandong, P.R. China, in 1985. Male. He received the bachelor‘s degree from Soochow University, P.R. China. He received the Master's degree from Hong Kong Polytechnic University. Now, he works in Hebei Institute of Communications. His research interest include fashion design, fashion merchandising and intelligent clothing.

Hangshuo Wu was born in shijiazhuang, Hebei, P.R.China, in 1993. Female.She received the Master degree from Beijing Institute of Fashion Technology, P.R. China. Now, she works in Hebei Institute of Communications, Her research interests include fashion design, Innovative clothing design, Digital clothing design.

References

[1] González-Lluch, C., Company, P., Contero, M., Camba, J. D., & Plumed, R. (2017). A survey on 3D CAD model quality assurance and testing tools. Computer-Aided Design, 83, 64-79.

[2] Li, C., Pan, H., Bousseau, A., & Mitra, N. J. (2022). Free2cad: Parsing freehand drawings into cad commands. ACM Transactions on Graphics (TOG), 41(4), 1-16.

[3] Kyratsis, P., Gabis, E., Tzotzis, A., Tzetzis, D., & Kakoulis, K. (2019). CAD based product design: A case study. Int J Mod Manuf Technol, 11(3), 110-5.

[4] Tzivelekis, C. A., Yiotis, L. S., Fountas, N. A., & Krimpenis, A. A. (2017). Parametrically automated 3D design and manufacturing for spiral-type free-form models in an interactive CAD/CAM environment. International Journal on Interactive Design and Manufacturing (IJIDeM), 11(2), 223-232.

[5] Tan, Q., & Li, H. (2024). Application of Computer Aided Design in Product Innovation and Development: Practical Examination on Taking the Industrial Design Process. IEEE Access, 12, 85622-85634.

[6] Wang, L. (2021, December). Computer Aided System Design of Fashion Design and Decoration Process under the background of Big Data. In 2021 5th International Conference on Electronics, Communication and Aerospace Technology (ICECA) (pp. 1691-1694). IEEE.

[7] Zheng, P. (2022). The CAD digital automation analysis of costume designing based on immersive virtual reality models. Advances in Multimedia, 2022(1), 3416273.

[8] Shaker, K., & Khan, H. (2017). CAD for textile fabrics. In Structural Textile Design (pp. 13-28). CRC Press.

[9] Yuan, Y., & Huh, J. H. (2018). Customized CAD Modeling and design of production process for one-person one-clothing mass production system. Electronics, 7(11), 270.

[10] Hasan, S. S. M. (2019). A comparative study on the role of fashion drawings for the design of women's clothing using CAD technology. International Design Journal, 9(4), 375-390.

[11] Hwang, C., & Zhang, L. (2020). Innovative sustainable apparel design: Application of CAD and redesign process. In Sustainability in the Textile and Apparel Industries: Sustainable Textiles, Clothing Design and Repurposing (pp. 87-107). Cham: Springer International Publishing.

[12] Jing, F., & Gui, Y. (2021, November). Research of Computer Aided Costume Design Application with Image Processing and Drawing Software. In Journal of Physics: Conference Series (Vol. 2083, No. 4, p. 042048). IOP Publishing.

[13] Lee, A. L., & Han, H. (2024). A review of parametric clothing pattern CAD software methodology. International Journal of Clothing Science and Technology, 36(1), 102-116.

[14] Jhanji, Y. (2018). Computer-aided design—garment designing and patternmaking. In Automation in garment manufacturing (pp. 253-290). Woodhead Publishing.

[15] Jankoska, M. (2020). Application CAD methods in 3D clothing design. Tekstilna industrija, 68(4), 31-37.

[16] Mohamed, S. M. (2025). The benefits of using 3D CAD software to modify clothing virtual prototype. International Design Journal, 15(2), 415-426.

[17] Dai, X., & Hong, Y. (2024). Fabric mechanical parameters for 3D cloth simulation in apparel CAD: A systematic review. Computer-Aided Design, 167, 103638.

[18] Chen, L., & Tong, Z. (2024). Innovation in Fashion Process Visualization Based on Parameterized CAD System. Computer-Aided Design and Applications, 215-228.

[19] Rahman, M. M., Ahmed, S., Mia, R., Shuva, I. B., Rahman, M. M., Ahammed, M. F., & Deng, Z. (2023). CAD technology aided design and evaluation of performance parameters of warp knitted seamless garment. International Journal on Interactive Design and Manufacturing (IJIDeM), 17(2), 787-799.

[20] Li, X., & Hou, W. (2023, September). Research on the Application of 3DMAX Integrated Computer Software in User Clothing Design System. In 2023 IEEE 6th International

Conference on Information Systems and Computer Aided Education (ICISCAE) (pp. 361-365). IEEE.

[21] Li, Y. (2022). Application and Development of Computer-Aided Design Methods in Clothing Design under the Environment of Internet of Things. Mobile Information Systems, 2022(1), 3405540.

[22] Jamil, Z., & Ijaz, M. (2024). Abstract Art as an Inspiration to Create Textile Patterns through Computer Aided Designing. Proceedings of the Pakistan Academy of Sciences: A. Physical and Computational Sciences, 61(2), 203-216.

[23] Hu, L. (2021). Design and Implementation of a Component-based Intelligent Clothing Style CAD System. Computer-Aided Design & Applications, 18.

[24] Liu, J. (2023). Application and research of computer aided technology in clothing design driven by emotional elements. International Journal of System Assurance Engineering and Management, 14(5), 1691-1702.

[25] Chen, F., & Zang, G. (2024). Data Mining-based Optimized Pattern Design and Color Scheme in Planar CAD. Computer-Aided Design and Applications, 21, 148-163.

[26] Wang, W., & Chen, L. (2024). Design and Implementation of Aerospace Arisa Fashion Design CAD System Based on Deep Convolution Neural Network. Computer-Aided Design & Applications, 21, 132-145.

[27] Lina Guo, Xueqin Sun, Yu Li, Sukai Wang & Ping Chen. (2025). Radial basis function-assisted global + local optimization algorithm for polarization-maintaining hollow-core anti-resonant fiber. Optics express,33(11),23075-23094.

[28] Addepalli V. N. Krishna & Addepalli Hari Narayana. (2017). Cubic spline curve public key cryptography. Journal of Discrete Mathematical Sciences and Cryptography, 20(2), 453-461.